energies

MDPI

Article

Microscopic Remaining Oil Classification Method and Utilization Based on Kinetic Mechanism

Yuhang He [1,*], Xianbao Zheng [1], Jiayi Wu [1,*], Zhiqiang Wang [1], Jiawen Wu [2], Qingyu Wang [1], Wenbo Gong [3] and Xuecong Gai [4]

[1] Exploration and Development Research Institute, Daqing Oilfield Company Limited, PetroChina, Daqing 163712, China; zhengxianbao@petrochina.com.cn (X.Z.); yjywangzhq@petrochina.com.cn (Z.W.); qingyuwang@petrochina.com.cn (Q.W.)
[2] Department of Energy Strategic Studies, Research Institute of Petroleum Exploration and Development, Beijing 100083, China; wujiawen@petrochina.com.cn
[3] College of Safety and Ocean Engineering, China University of Petroleum, Beijing 102249, China; wenbog@163.com
[4] The 7th Oil Production Plant of Daqing Oilfield Company Ltd., PetroChina, Daqing 163000, China; gaixuecong@petrochina.com.cn
* Correspondence: hyuhang@petrochina.com.cn (Y.H.); wujiayi@petrochina.com.cn (J.W.); Tel.: +86-15304597505 (Y.H.); +86-13704595772 (J.W.)

Abstract: In reality, the remaining oil in the ultra-high water cut period is highly dispersed, so a thorough investigation is required to understand the microscopic remaining oil. This will directly influence the technological direction and allow for countermeasures such as enhanced oil recovery (EOR). Therefore, this study aims to investigate the state, classification method and utilization mechanism of the microscopic remaining oil in the late period of the ultra-high water cut. To achieve this, the classification of microscopic remaining oil based on mechanical mechanism was developed using displacement CT scan and micro-scale flow simulation methods. Three carefully selected mechanical characterization parameters were used: oil–water connectivity, oil–mass specific surface and oil–water area ratio. These give five types of microscopic remaining oil, which are as follows: A (capillary and viscous oil cluster type), B (capillary and viscous oil drop type), C (viscous oil film type), D (capillary force control throat type), and E (viscous control blind end type). The state of the microscopic remaining oil in classified oil reservoirs was defined after high-expansion water erosion. Based on micro-flow simulation and analysis of different forces during the displacement process, the main microscopic remaining oil recognized is in class-I, class-II and class-III reservoirs. Within the Eastern sandstone oilfields in China, the ultra-high water-cut stage is a good indicator that the class-I oil layer is dominated by capillary and viscous oil drop types distributed in large connected holes. The class-II oil layer has capillary and viscous force-controlled clusters distributed in small and medium pores with high connectivity. In the case of the class-III oil layer, it enjoys the support of capillary force control throats that are mainly distributed in small holes with high connectivity. Integrating mechanisms of different types of micro-remaining oil indicates that, enhancing utilization conditions requires increasing pressure gradient and shear force while reducing capillary resistance. An effective way to improve the remaining oil utilization is to increase the pressure gradient and change the flow direction during the water-drive development process. Hence, this forms a theoretical basis and a guide for the potential exploitation of remaining oil. Likewise, it provides a strategy for optimizing enhanced oil recovery in the ultra-high water-cut stage of mid-high permeability oil reservoirs worldwide.

Keywords: microscopic remaining oil; pore types; displacement analysis; CT scanning; oil classification; occurrence state; utilization mechanism

Citation: He, Y.; Zheng, X.; Wu, J.; Wang, Z.; Wu, J.; Wang, Q.; Gong, W.; Gai, X. Microscopic Remaining Oil Classification Method and Utilization Based on Kinetic Mechanism. *Energies* **2024**, *17*, 5467. https://doi.org/10.3390/en17215467

Academic Editor: Shu Tao

Received: 12 August 2024
Revised: 15 October 2024
Accepted: 23 October 2024
Published: 31 October 2024

1. Introduction

Although most of China's mid–high-permeability old oil fields have entered the ultra-high water cut stage, they are confronted with several challenges such as high water cut, low recovery rate and difficulty in tapping remaining oil [1–4]. Similarly, how to determine the distribution and law guiding saturation of remaining oil are key issues in realizing the deep development of remaining oil for efficient oil recovery [5]. At present, preferential seepage channels are formed in the pores of long-term producing reservoirs, resulting in inefficient and ineffective circulation of water injection, and difficulty in effectively recovering remaining oil [6,7]. Getting the oil that is not affected by water in the micro-pore space is the main object of potential exploitation in the ultra-high water cut period [8,9]. Thus, its distribution characteristics and effective exploitation need to be further studied.

In recent years, the methods used to study the microscopic remaining oil include glass etching, laser confocal, digital core simulation, etc. [10–17]. Combined with imaging techniques, the occurrence state of remaining oil was identified within porous space. Previous works focused mainly on the classification of types based on morphological characteristics with few studies on stress characteristics and utilization mechanism of microscopic remaining oil [18–25]. Jia et al. [26] divided the occurrence and location of the microscopic remaining oil distribution using a two-dimensional planar microscopic visualization model experiment. The five types of microscopic remaining oil identified were: cluster, granular, throat, blind end, pore membrane and particle adsorption. Going by this division, although the distribution characteristics of the microscopic remaining oil were revealed, their formation mechanism and utilization conditions were not discussed. Bai et al. [27] used laser confocal experiments to divide the main causes, existence forms and distribution patterns of the microscopic remaining oil into two main genetic types: pore throat difference and particle adsorption. The authors also established the existence of three forms (free state, semi-bound state and bound state), which were further subdivided into 10 distribution patterns. Furthermore, based on the morphological characteristics (shape factor and contact area ratio), Li et al. [28] used the shape factor, contact area ratio and pore throat number to further divide the microscopic remaining oil into oil film, oil droplet, columnar oil, porous oil and cluster oil. Although these studies provided a preliminary understanding of the formation and utilization of the micro-remaining oil at the pore scale, they do not consider the micro-stress factors. Gong et al. [29] identified the stress characteristics of the microscopic remaining oil in mid-high permeability reservoirs based on core simulation experiments and divided them into five types. However, the research was based on the pore structure model with a simple structure which did not specifically discuss the types of remaining oil found in actual production (such as corner and blind end). Coincidentally, the distribution characteristics of remaining oil under different pore structure characteristics were not considered. This is an important factor that determines the actual development of oil fields in the ultra-high water cut period hence, cannot be left out.

As a typical continental sandstone oilfield in China, the LaSaXing (LSX) oilfield is in the stage of high water cut post-development having highly dispersed remaining oil, with water and chemical flooding as the main methods of displacement. The fact that the dominant flow within the reservoir and remaining oil coexist makes it increasingly difficult to tap the remaining oil [30]. In effect, understanding the microscopic interfaces and the state of microscopic remaining oil distribution is crucial to enhance oil recovery in the high water cut post-development stage. Currently, this accounts for the two main technical problems in this field.

Firstly, the microscopic morphology, distribution position and type of remaining oil in the high water cut post-development stage directly affect the choice of further exploitation methods. Thus, there is a need to identify the microscopic remaining oil distribution state. Secondly, different types of microscopic remaining oil have different mechanisms of force application and mobilization conditions. Understanding their mobilization conditions is crucial for further exploitation.

In this paper, four core samples from different mid-high permeability reservoirs in the LaSaxing oilfield of the Daqing Placanticline in the northern Songliao Basin were subjected to systematic studies. This includes CT-scan of different sizes, high-precision CT-scan with displacement and mercury injection at a constant rate. Integrating the types of remaining oil found in actual development makes it easy to classify the microscopic remaining oil based on its dynamic features which was optimized to clarify the different stress types. By subdividing the micro-pore structure, it was possible to define the state of micro-remaining oil for different reservoir types in the late period of ultra-high-water cut. From this information, the evolution mechanism of different types of micro-remaining oil as well as the conditions for the utilization of remaining oil were clarified. This indeed assists in determining the effective means to improve the utilization degree of micro-remaining oil. Therefore, these lay a theoretical foundation to further enhance oil recovery in the later period of ultra-high water cut.

2. Displacement Experiment

To understand the state of the microscopic remaining oil in the late ultra-high water cut, an integrated CT scan involving core displacement of class-I, class-II and class-III reservoirs was used in this study. The analysis will assist in broadening the understanding of the law guiding microscopic remaining oil distribution at different development stages [31,32].

2.1. Sample Selection

The sample selection in this study considered the fact that different oil layers have different pore structures, degrees of utilization and distributions of residual oil. Hence, classified oil layer sampling was adopted in this study. To ensure the best scanning effect, sample permeability, porosity, median particle size and other parameters were provided. This was done to determine the shaping scheme of class-I, class-II and class-III reservoirs as well as the off-sheet representative sand body. The sample was about 2.5–5.0 cm long with a diameter of 2.5 cm, while the specific accuracy requirements of different oil layers are as defined in Table 1. The class-I layer is selected from the top and bottom of the large channel sand body. Based on the design, the top and bottom air permeabilities should not be less than 800 mD and 3000 mD, respectively. Meanwhile, the top and bottom of the middle/small class-II reservoir sand were selected by considering samples with about 300 mD and 1000 mD for the top and bottom, respectively. Going by this principle, 4 representative samples (1, 2, 3 and 4) were carefully selected for the analysis.

Table 1. Requirements for sample size and resolution.

Reservoir Type	REV Analysis	CT Scanning	
		Rough Scanning	Fine Scanning
Class-I	Diameter = 2.0–2.5 cm, Length = 3.0–5.0 cm	Size: Diameter = 2.5 cm, Length = 2.5–5.0 cm Resolution: 5 μm	Size: Diameter = 8 mm, Length = 8 mm, Resolution: 4 μm
Class-II			Size: Diameter = 8 mm, Length = 8 mm, Resolution: 4 μm
Class-III			Size: Diameter = 8 mm, Length = 8 mm, Resolution: 2 μm

Before the experiment, 4 core samples of different reservoirs were cleaned with gasoline. A cable extraction device is used to wash the oil, and a round-bottom flask containing chemical reagents is placed in the heating furnace. When the temperature reaches the boiling point, the reagent evaporates to form steam, and the steam rises to the condensing tube and condenses into liquid drops into the sample chamber. When the liquid level in the sample chamber reaches the siphon point, the reagent is returned to the bottom of the flask, and the process is repeated to rinse the sample repeatedly until all pore fluids are removed. The cleaning agent is gasoline.

The porosity and permeability of the samples were measured using an ESK-III core permeability tester (Wuxi Huiao Instrument, Ltd., Wuxi, China), electronic balance (Sartorius Scientific Instruments, Ltd., Beijing, China) and KX-90G compact vacuum saturation device (Jiangsu Huaan Instrument, Ltd., Nantong, China) according to the "Practices for core analysis" standard (GB/T 29172-2012) [33].

In the porosity measurement process, helium is injected into the reference chamber with the volume V1 and the equilibrium pressure is P1. After opening the valve, helium gas enters the sample chamber of container V2, which has a rock with a skeleton volume of Vg. There is a rock with a skeleton volume of Vg in the sample chamber, and the equilibrium pressure is P2. Under the premise of stable room temperature, the skeleton volume of the sample can be calculated according to Boyle's law P1V1 = P2 (V1 + V2 − Vg). The effective porosity of the sample can be calculated by measuring the total volume with calipers or buoyancy method.

A steady-state permeability meter is used to measure rock permeability according to Darcy's law of stable gas seepage, reflecting the ability of gas to pass through porous rock under the action of pressure difference. Using compressed air or nitrogen as the medium, according to Darcy's law, the volume velocity of fluid passing through porous media per unit cross-sectional area is proportional to the potential energy gradient and inversely proportional to the viscosity of fluid.

$$K = (Q \times \mu \times L) \div (P1 - P2) \times S$$

wherein:

K—Core permeability (μm);
Q—Flow (mL/s);
μ—Viscosity (Pa·s);
P1—Balanced pressure P1 (Mpa);
P2—Balanced pressure P2 (Mpa);
L—Core length (cm);
S—Core cross sectional area (cm^2).

Details of the sample porosity and air permeability parameters are presented in Table 2.

Table 2. Basic reservoir parameters of the core samples.

Sample	Reservoir Type	Lithology	Porosity (%)	Air Permeability ($\times \mu m^{-3}$)
Sample-1	Class-I	fine-grained sandstone	30.96	3956
Sample-2	Class-I	fine-grained sandstone	29.32	1890
Sample-3	Class-II	fine-grained sandstone	28.84	1398
Sample-4	Class-III	siltstone	27.79	462

2.2. Experimental Condition

Advanced core displacement and high-precision CT scanning equipment were used in this study. A non-destructive 3D X-ray microfocus computed tomography system, along with a high-pressure, high-precision plunger pump and customized core holding, were utilized. This was used with the Xradia MicroXCT-400 micro-CT (Xradia, Inc., Pleasanton, CA, USA), which has a maximum resolution of <1 μm. This gives full interior details of large samples in a 3D panorama as it enables high-resolution and high-contrast imaging for small samples while using large geometric magnifications. Since 4 mm is required for the core displacement analysis, a special gripper was developed. During the process, a small core plug of 4 mm in diameter and about 8 mm long was produced using wire-cutting technology. The core was put into the core gripper for oil-water displacement analysis (Figure 1). Teledyne ISCO high-pressure high-precision piston pump 500D (Teledyne ISCO, Lincoln, NE, USA) was employed for flow control. This is to allow the solvent in the pump

to attain 507 mL and a desired pressure of 10–3750 psi. Experimental flow rates vary from single (0.001–204 mL/min) to double pump continuous flow (0.001–133 mL/min) at a set accuracy of 0.5%, drive resolution 31.71 nL (Figure 2).

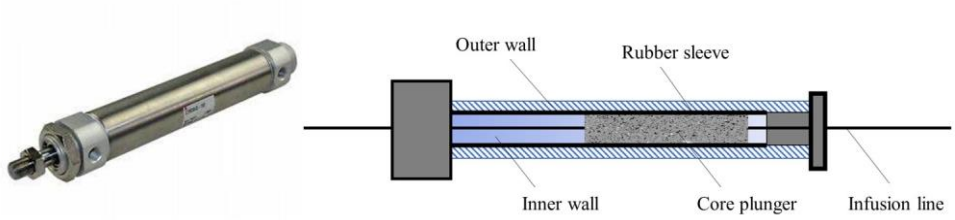

Figure 1. Customized 4 mm core holder (**left** picture) and internal structure (**right** picture).

Figure 2. ISCO high-pressure high-precision piston Pump 500D.

2.3. Experimental Procedure

Four (4) representative core samples were subjected to displacement simulation experiments using different water flooding conditions at constant pressure and temperature. The CT scan was performed at 8 designed nodes, while quantitative values of microscopic remaining oil were computed at each displacement node for each sample (Figure 3, Table 3). Also, the fluids used for displacement were the crude oil and water produced from the development block in the Daqing oilfield. The surface viscosity and API gravity of crude oil were about 12.8 and 33.8, respectively, and the salinity of water produced was about 7200 mg/L.

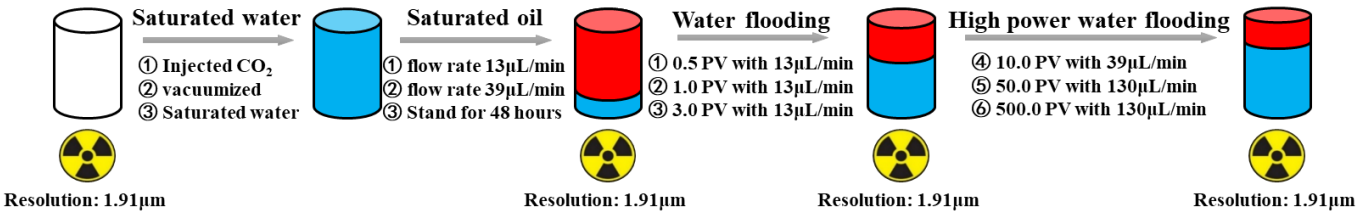

Figure 3. Schematic diagram of water drive experiment node design.

Table 3. Scanning nodes in high-precision CT scanning experiments of different displacement coordination methods.

Node	Node 1	Node 2	Node 3	Node 4	Node 5	Node 6	Node 7	Node 8
Degree	Dry Rock	Oil-Saturated	0.5 PV with 13 μL/min	1 PV with 13 μL/min	3 PV with 13 μL/min	10 PV with 39 μL/min	50 PV with 130 μL/min	500 PV with 130 μL/min

3. Occurrence of Micro Remaining Oil

In this study, the displacement experiment was carried out on 4 selected samples to define their characteristics. For sample-1, the result shows that an increase in the degree of displacement leads to a change in the remaining oil from centralized flake to scattered and isolated distribution (Figure 4). This brings about a decrease in the saturation of the remaining oil from 74.4% to 18.46%. In terms of classified oil layers, the result reveals a rapid change in the Class-I recovery compared to gradual and small changes recorded for Class-II and Class-III (Figure 5). Furthermore, a reasonable change in the pore volume (3 PV to 10 PV) was noted as the displacement velocity rose from 13 μL/min to 39 μL/min, leading to a significant rise in recovery. Figure 5 illustrates how the displacement efficiency increased from 10 to 50 PV before the reservoirs showed very low recovery after 50 PV. This indicates that there is a need to further evaluate the principles guiding the micro-remaining oil evolution at different water flooding stages. Based on the result of this study, it is clear that the distribution type, location and oil-control mechanism of micro-remaining oil are important factors to be considered when analyzing the oil characteristics.

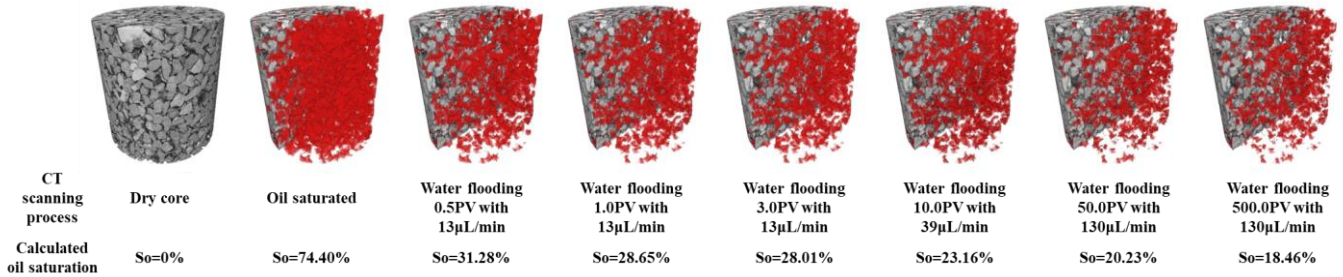

Figure 4. Distribution of remaining oil in sample-1 at different displacement nodes (Red color: remaining oil).

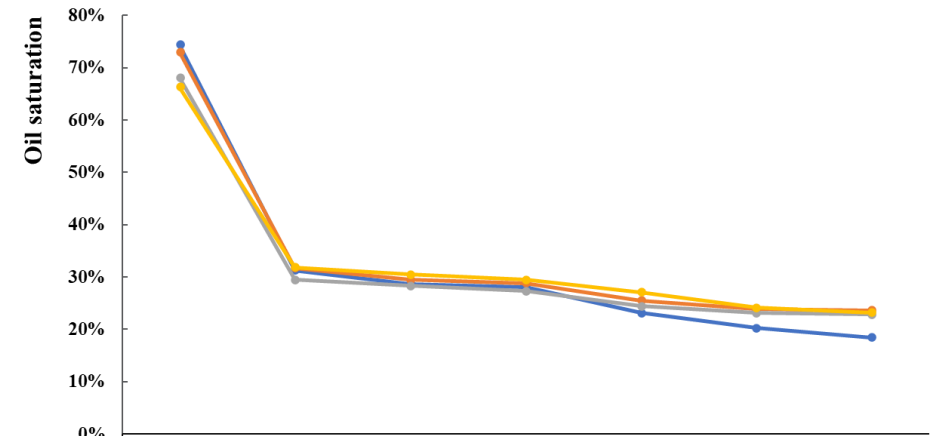

	Oil-saturated	0.5PV with 13μL/min	1.0 PV with 13μL/min	3.0 PV with 13μL/min	10.0 PV with 39μL/min	50.0 PV with 130μL/min	500.0 PV with 130μL/min
Sample-1	74.40%	31.28%	28.65%	28.01%	23.16%	20.23%	18.46%
Sample-2	73.00%	31.70%	29.49%	28.86%	25.54%	23.88%	23.61%
Sample-3	68.12%	29.47%	28.32%	27.34%	24.41%	23.11%	22.87%
Sample-4	66.30%	31.84%	30.47%	29.49%	27.06%	24.14%	23.19%

Figure 5. Change in reservoir production.

To explain the occurrence of microscopic remaining oil, the core displacement data was utilized to classify the remaining oil types based on the microscopic stress mechanism. This was done to define the formation mechanism and distribution of microscopic remaining oil to provide a theoretical background for accurate potential exploration in the later high water cut.

3.1. The Classification Method

The traditional method of classifying microscopic remaining oil has been based on morphological characteristics. This includes cluster, in-grain, throat, blind end, pore membrane and particle adsorption, etc. [34–36]. It is good to note that, previous studies do not consider the microscopic stress factors and fail to explore the main stress characteristics of microscopic remaining oil from a dynamic perspective. As a result, there is still a poor understanding of the formation mechanism of microscopic remaining oil. Therefore, this paper starts from the microscopic force, and conducts in-depth research on the mechanical mechanism, parameter selection, boundary determination and other aspects. In effect, it builds a classification method of microscopic remaining oil based on mechanical mechanism.

3.1.1. Classification Parameter Optimization

At the pore scale, the main microscopic forces acting on micro cluster fluids are capillary force, viscous force, positive pressure, gravity and inertia force. This involves 4 dimensionless parameters which are Bond number, Froude number, Reynolds number and capillary number. These parameters were used to evaluate the relative strength between gravity and capillary force, inertia force and gravity, inertia force and viscous force as well as viscous force and capillary force. The following are the calculation results:

$$\text{Bond number}: \ Bo = \frac{\Delta\rho g R^2}{\sigma} \approx 10^{-4}$$

$$\text{Froude number}: \ Fr = \sqrt{u^2/gR} \approx 10^{-4}$$

$$\text{Reynolds number}: \ Re = \frac{\rho u R}{\mu} \approx 10^{-5}$$

$$\text{Capillary number}: \ Ca = \frac{\mu u}{\sigma} \approx 10^{-6}$$

where:

Waterflood displacement rate, $u = 11$ μm/s;
Mean pore radius, $R = 50$ μm;
Water phase density, $\rho_w = 1000$ kg/m^3;
Oil phase density, $\rho_o = 850$ kg/m^3;
Surface tension of water and oil, $\sigma = 30$ mN/m;
Oil phase viscosity, $\mu_o = 10$ mPa·s.

Judging from the formulas above, the Bond and Froude numbers show that the inertia force and gravity are relatively weak compared to the capillary force during the stress process of the oil. The Reynolds and capillary numbers show that the capillary force plays a dominant role as the microscopic force, while the viscous force is stronger than the inertial force. Therefore, the analysis focuses on the microscopic remaining oil in the digital pore structure with positive pressure, viscous force and capillary force of three major microscopic force processes. A typical example of this type of force is shown in Figure 6.

To clearly define the remaining oil, this study explores and analyzes all the possible forces based on a dynamic balance perspective. In principle, each microscopic force may be the driving force of the microscopic remaining oil but also constrain the movement of the oil to a certain extent. Therefore, to have a clear picture of the combined triangular force distribution in Figure 6, each micro-force form was analyzed and the result is shown in Table 4.

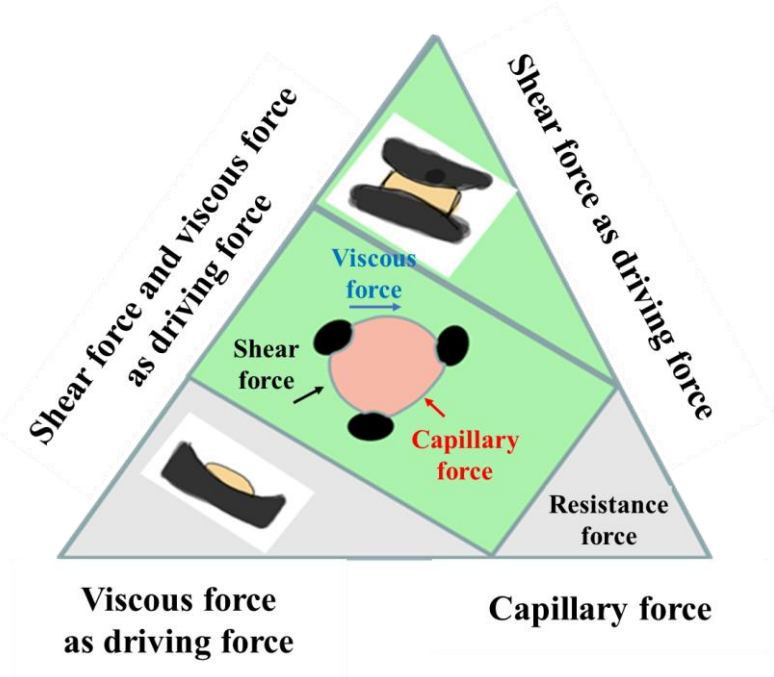

Figure 6. Ideal stress form of micro remaining oil.

Table 4. Forces controlling micro remaining oil.

Type	Driving Force	Resistance Force
1	Positive pressure	Capillary force
2	Positive pressure	Viscous force
3	Viscous force	Positive pressure
4	Viscous force	Capillary force
5	Capillary force	Positive pressure
6	Capillary force	Viscous force
7	Viscous force, positive pressure	Capillary force
8	Capillary force, viscous force	Capillary force
9	Capillary force, positive pressure	Viscous force
10	Capillary force	Positive pressure, viscous force
11	Viscous force	Positive pressure, capillary force
12	Positive pressure	Viscous force, capillary force

Based on the dynamic equilibrium analysis of each of the forces, it can be observed that if the capillary force is the driving force, its microscopic force state is imbibition as shown in Figure 7a. This is a case where the water phase is constantly driven by the capillary force to transport the oil phase, which makes it difficult to form a stable remaining oil distribution. When the viscous force is the driving force with positive pressure as the resistance, the conceptual force model is shown in Figure 7b. Under the combined action of viscous shear and positive pressure, the oil phase is distorted until part of the oil phase is removed. This leads to weakening of the positive pressure and the microscopic remaining oil develops capillary force as the resistance. Therefore, the microscopic force distribution will result in force imbalance. The microscopic force with positive pressure as the driving force and viscous force as the resistance occurs mainly in the process of internal flow of single-phase fluid (Figure 7c). Positive pressure drives fluid movement, resulting in viscous dissipation and pressure loss within the fluid. This does not apply to the force analysis of

microscopic remaining oil. Furthermore, having positive pressure as the driving force and capillary force as the resistance indicates that, the viscosity of the microscopic remaining oil is extremely weak with no viscous shear between the two phases of fluid. This force type is typical of the water-oil displacement process in large channels (Figure 7d). In this case, the oil phase moves continuously under positive pressure until it breaks away from the constraint of the pore structure. Therefore, this force does not apply to the microscopic remaining oil in the digital core with pore structure as obtainable in this work.

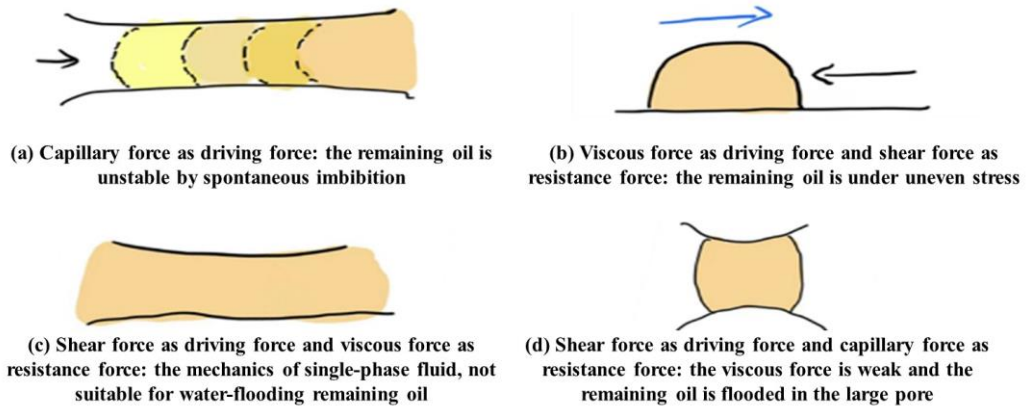

Figure 7. Ideal microscopic stress form of remaining oil and its conceptual model.

The results show that three mechanisms keep the microscopic remaining oil in equilibrium condition. By analyzing all the ideal forces controlling the microscopic remaining oil in the pore structure, these are: (1) the viscous (driving) force and the capillary (resistant) force (2) positive pressure (driving force) with viscous and capillary forces as resistant component, and (3) the viscous force and positive pressure are the driving forces which are restrained by the capillary force. Under these three conditions, the capillary force serves as a resistance to control the migration of micro-remaining oil. Therefore, in the classification of micro-remaining oil based on force type, the conceptual models are established from the perspective of the dynamic balance of micro-remaining oil. Similarly, three parameters that have been established to be key in characterizing the micro-remaining oil are water–oil interface connectivity, oil–body surface area and water–oil area ratio. These are closely related to the force types and can be easily obtained.

Water–oil interface connectivity refers to the number of water interfaces in contact with the microscopic remaining oil. This represents the potential flow direction of the remaining oil migration in the process of water flooding and reflects the swept capacity of injected water. Based on this, the widely distributed cluster of microscopic remaining oil can be distinguished from the microscopic remaining oil in the local pore structure.

Oil–body surface area denotes the ratio of the surface area of the microscopic remaining oil to the volume of the microscopic remaining oil. This indicates the form of microscopic forces on the surface of the remaining oil in the pore structure. Note that, when the value is small, the microscopic remaining oil is mainly subjected to a single dynamic action, and its shape is inclined (flat). On the other hand, if the value is large, the microscopic remaining oil is subjected to combined dynamic action leading to the formation of remaining oil in oil droplets.

Water–oil area ratio is a term for the ratio of the water-oil surface area to the microscopic remaining oil surface area. This represents the dominant driving force in the process of dynamic equilibrium. If the viscous force is the dominant force, the value is relatively large, but when the positive pressure is the dominant force, the value is relatively small.

The correlation between the force and the microscopic occurrence state was clarified according to the force analysis of the microscopic remaining oil. On this basis, the method of characterizing the microscopic remaining oil with three parameters was innovatively established.

This is to lay the foundations for quantitative characterization of the forces and distribution of the microscopic remaining oil in the digital core model at different displacement stages.

3.1.2. Classification of Boundary Determination

Based on the force analysis and morphological statistical characteristics of the microscopic remaining oil, the "rich" and "barren" areas which are greatly different from the mainstream were analyzed. This is to determine its mechanical characteristics as the key to classifying the remaining oil types [37].

In this study, the Kernel Density method was adopted to determine the critical value of remaining oil morphology. Apart from the demarcation point, two data sets were provided for the study. The probability significance of the two data sets was evaluated by determining their demarcation point such as the mechanical and statistical characteristics of microscopic remaining oil (see the green dashed line in Figure 8). In Figure 9, the comparative analysis of the significance difference indicates that the correlation between the left and right data sets is weak. This is because the left and right data sets no longer change and are at low values. The side with most samples represents the main morphological characteristics and force mode of the core micro-remaining oil. This method is used to establish the boundaries of "water-oil interface connectivity", "water-oil area ratio" and "Oil-body surface area" after the 0.5 PV displacement. These are used in classifying the micro-remaining oil types.

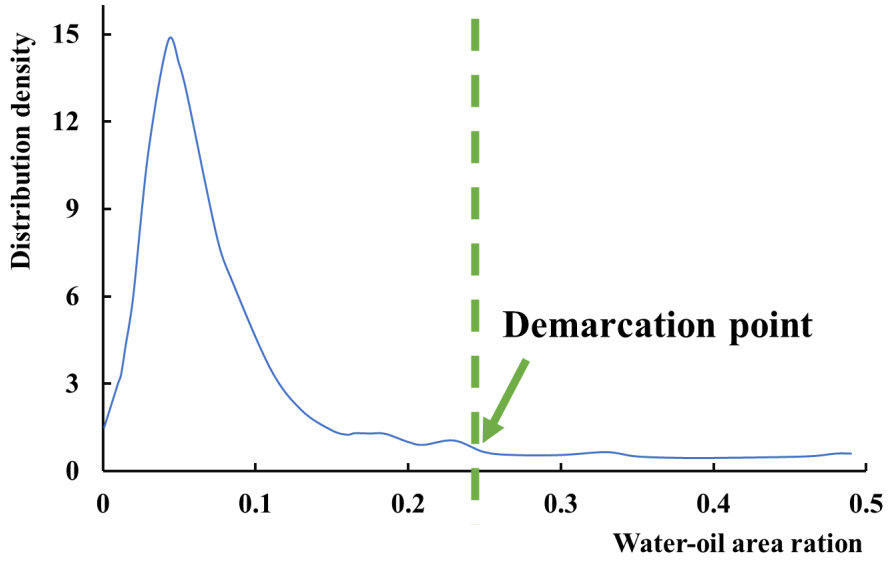

Figure 8. Density distribution curve of the remaining oil–water–oil area ratio.

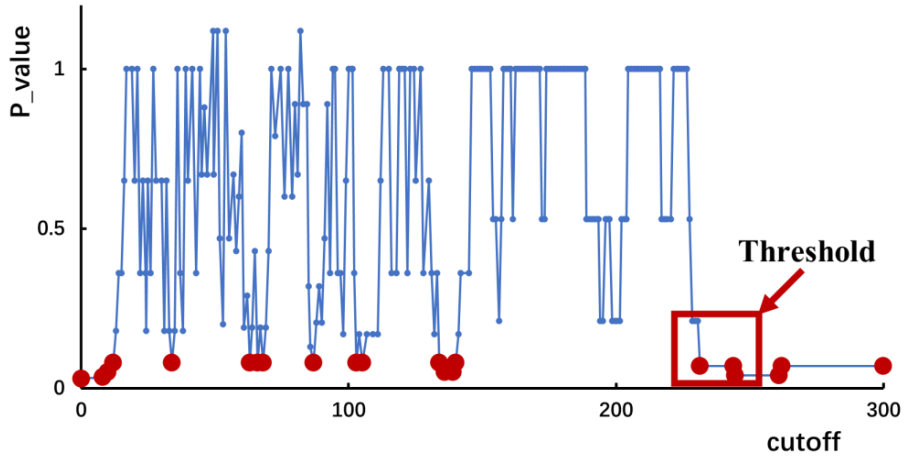

Figure 9. *p*-value distribution of the water–oil area ratio.

3.1.3. Types of Microscopic Remaining Oil

Based on the water-oil interface connectivity, the pore structure can be divided into high connectivity and low connectivity. The high connectivity type belongs to the porous type with capillary + viscous force-controlled cluster type, which is mainly characterized by multi-force. As for the low connectivity type, it is generally a single oil droplet. The remaining oil of low connectivity single oil droplets can be further subdivided into high and low specific surfaces according to the oil-body surface area. Meaning that the lower the specific surface, the more spherical it tends to be. This is mainly controlled by capillary + viscous forces and is defined as the oil droplet controlled by capillary and viscous forces. The higher the specific surface, the more flat or cylindrical it tends to be. The remaining oil with a low water-oil area ratio is mainly dominated by capillary force and is defined as a cylindrical shape controlled by capillary force. In contrast, the remaining oil having a high water-oil area ratio is flat or irregular with a blind end shape dominated by viscous force. This is often defined as the blind end and oil film type controlled by viscous forces.

Going by the above research, a classification method combining microscopic forces and morphological characteristics of microscopic remaining oil types was used to establish five types of controlling force as follows (Figure 10), and all types of remaining oil could be found in the 3D digital cores of samples (taking Sample-2 as an example in Figure 10):

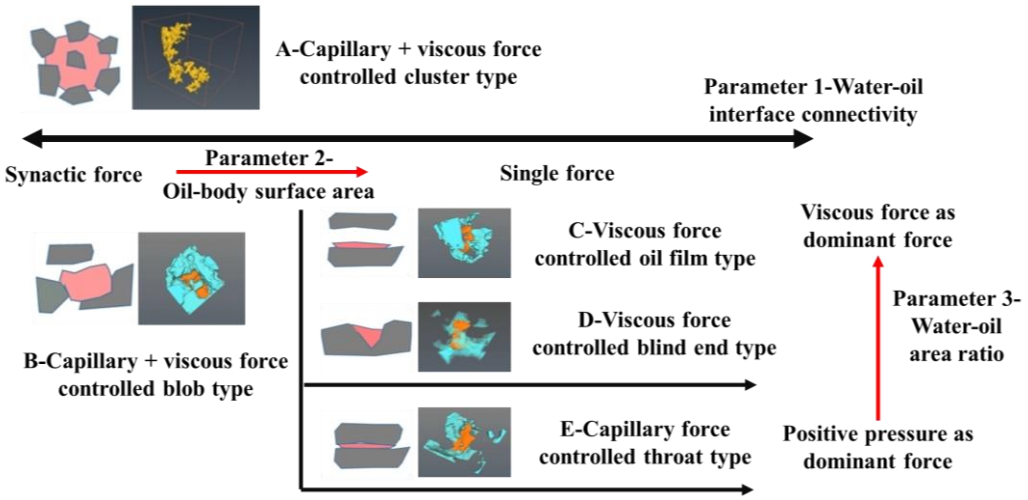

Figure 10. Classification of remaining oil types based on mechanical analysis (taking Sample-2 as an example).

A-Capillary + viscous force-controlled cluster type. It mostly forms in areas where the displacement agent is not swept or in the pore space where the oil-displacing agent is hard to get as a result of the dynamic balance at the oil-water interface. This is caused by the complex "pointing" phenomenon in the core at the early stage of the water flooding process. The force (type A) is complex as it involves multiple microscopic forces. By the nature of this force, it is clear that the main driving force comes from positive pressure occupying multiple pores with wide spatial distribution.

B-Capillary + viscous force-controlled blob type. This case is common in places where the oil-water interface area is large, and the water phase appears to follow the "flow around" phenomenon. The micro-remaining oil surface associated force type A involves a combined mechanism of positive pressure as a displacing force and viscous force as a shearing force. The Type B micro-remaining oil is enriched in the mechanical mode of viscous force and positive pressure as the displacing force and capillary force as the resistance. Note that, the viscous force is the dominant driving force. This type of microscopic remaining oil most often presents an elliptical shape with a smaller surface area affected by the viscous and capillary force.

C-Viscous force-controlled oil film type. The remaining oil volume of this type is small but has a relatively large surface area. This translates to a relatively large force area for the oil-water interface. The displacement agent spreads on the surface of the microscopic remaining oil, despite the weak positive pressure displacement. Thus, the distribution is planar as the volume of a single microscopic remaining oil is small.

D-Viscous force-controlled blind end type. This is characterized by a small specific surface with a single area of oil-water interface. The connectivity parameters are constant. Under this force type, the microscopic remaining oil is more constrained by the capillary force, and the viscous force in the two-phase interaction area is limited. Thus, it is restricting the remaining oil migration. This means that this kind of microscopic remaining oil is subjected to the combined action of the viscous and capillary forces. It has to be stated that the capillary force still serves as the resistant force.

E-Capillary force-controlled throat type. In this case, the remaining oil volume is small but has a relatively large surface area. The force area of the oil-water phase interface is relatively small making the microscopic remaining oil to be constrained by the pore structure. This in effect will make it hard for the displacement agent to enter the pore structure to displace the remaining oil by positive pressure. In the process, the type D micro-remaining oil is enriched in the mechanical mode with positive pressure as the driving force and capillary force as the resistance. Typical examples of this are often distributed in narrow and long pore channels, where the capillary force is greater than the displacement power. Therefore, leading to the production of saturated pore structures.

3.2. State of Occurrence

Pore structure characteristics are one of the main factors controlling the distribution of microscopic remaining oil [38]. To define the dynamic distribution characteristics of remaining oil in different reservoirs, it is necessary to first classify the microscopic pore structure. As earlier mentioned, based on the fluid dynamic behavior in the pore structure, the pore flow capacity and connectivity are the main evaluation indexes. On this basis, the microscopic pore structure is divided into high-connectivity large pores, high-connectivity mid pores, high-connectivity small pores, low-connectivity large pores, low-connectivity mid pores and low-connectivity small pores. Knowing this, the distribution characteristics of the remaining oil types in different reservoirs' pore structures were extracted.

Evolution of class-I reservoir microscopic remaining oil. The fluid dynamic evolution based on the digital core of Sample-1 from the Class-I reservoir (Figure 11) shows that the Class-I reservoir is characterized by large pore size, high permeability and good pore connectivity. The initial remaining oil belongs to category A (capillary + viscous force-controlled cluster type) which is mainly distributed within high connectivity large pores. In the long-term water flooding process, the internal microscopic remaining oil is subjected to the joint action of positive pressure and viscous force. Under this condition, large positive pressure is developed along with a small viscous force, as the remaining oil in high connectivity pores is flushed easily. After establishing a stable dominant displacement path in the high connectivity large pore, the remaining oil in the high connectivity mid-small pore still has more B (capillary + viscous force-controlled blob type), Note that at this stage it is largely controlled by large capillary force, which makes it attains the equilibrium state more quickly. During the late period of high-water flushing, the volume and quantity change amplitude is weak and its volume accounts for about 72% of the total remaining oil after 500 PV (Figure 12).

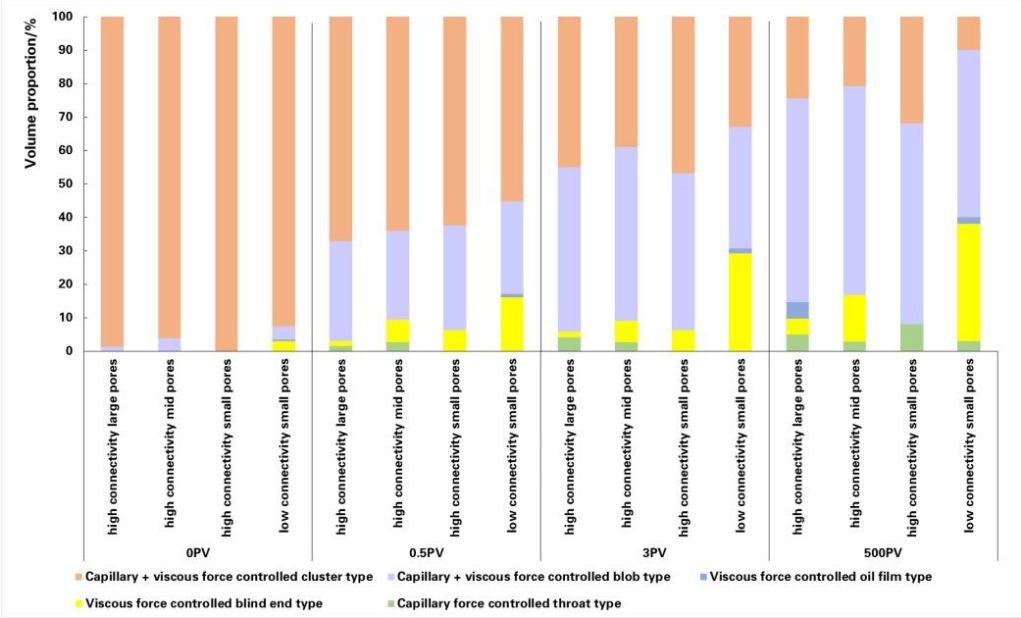

Figure 11. Evolution of microscopic remaining oil in class-I reservoir.

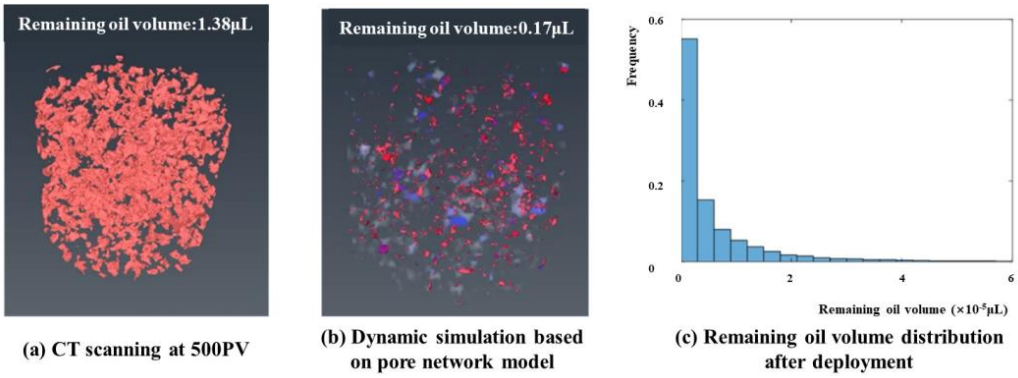

(a) CT scanning at 500PV

(b) Dynamic simulation based on pore network model

(c) Remaining oil volume distribution after deployment

Figure 12. Simulation of micro-remaining oil production in digital core of class-I oil reservoir.

Evolution of class-II reservoir microscopic remaining oil. The fluid dynamic evolution based on the digital core of Sample-2 from the Class-II reservoir (Figure 13), the experimental result shows that the class-II reservoir has large porosity, low pore diameter and relatively high permeability. However, the heterogeneity of the pore structure makes it difficult for the injected water to spread over a large area. In this way, the dominant path is easily formed in the course of long-term water flooding which results in an inefficient water flooding cycle. Therefore, the micro-remaining oil forms a porous continuous distribution of capillary + viscous force-controlled cluster (A-type). The remaining oil is distributed within the high-connectivity mid-small pores as the oil quantity gradually changes. It is good to note that, the increase in volume recorded after 0.5 PV accounts for 67.6% of the total remaining oil volume. Category D (viscous force controlled blind end type) is the second most common occurrence state which accounts for about 19.6%. With the change in the water drive ratio, the remaining oil in the high connectivity pores is more flooded. However, the water-sweep in the high connectivity mid-small pore is poor, leading to enrichment in the type-A remaining oil (Figure 14).

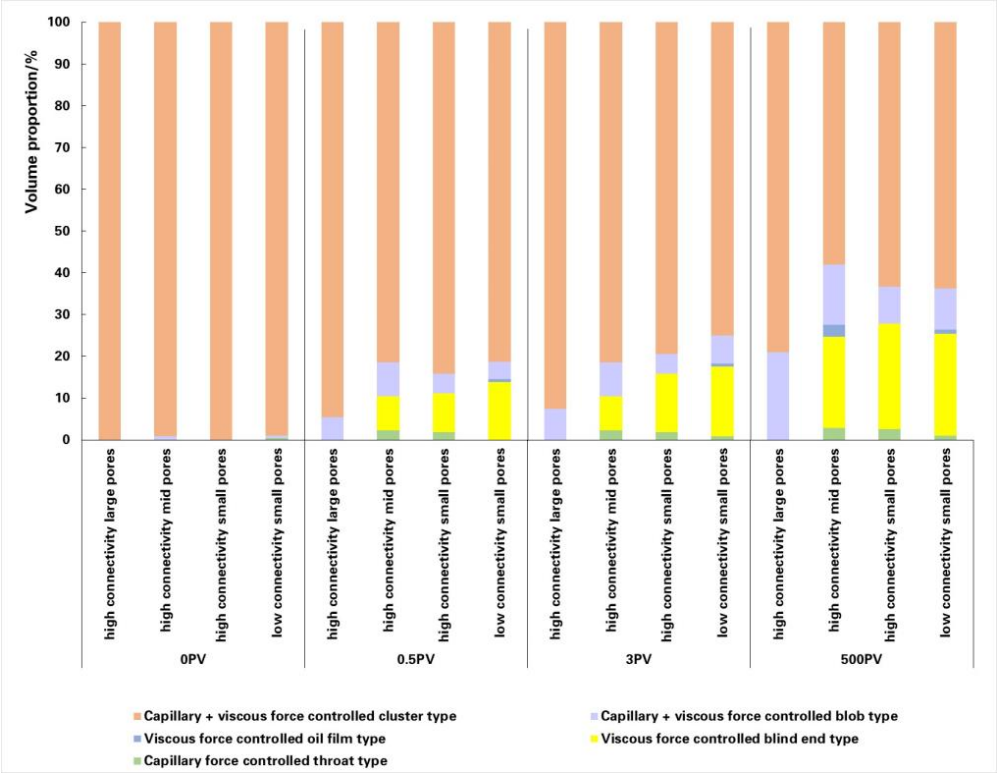

Figure 13. Evolution of microscopic remaining oil in class-II reservoir.

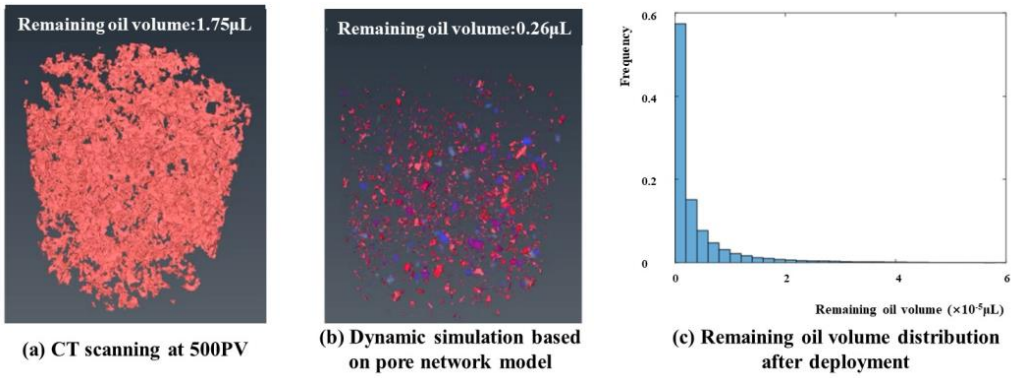

(a) CT scanning at 500PV (b) Dynamic simulation based on pore network model (c) Remaining oil volume distribution after deployment

Figure 14. Simulation of micro-remaining oil production in the digital core of class-II oil reservoir.

Evolution of class-III reservoir microscopic remaining oil. The fluid dynamic evolution based on the digital core of sample-4 from Class-III reservoir (Figure 15), class-III reservoir shows evidence of small pore size, low permeability and strong heterogeneity. This means that the microscopic remaining oil distributed in the pore is subjected to high capillary force. Both the spread range of injected water and the displacement efficiency experience a gradual increase. Also, during the long-term water flooding process, micro-remaining oil controlled by A-type was flushed and fragmented. In effect, the crushing process is affected by local pore structure bound by high capillary force. Since the positive pressure is not enough to overcome the resistance, it will form a sheet of remaining oil within narrow pores. This results in type D which is the viscous force-controlled blind end type. The amount of type-D remaining oil increased continuously in the process of high-water flooding, indicating that it was mainly converted from other types of microscopic remaining oil. Therefore, its volume accounted for about 49.8% of the total remaining oil volume after 500 PV (Figure 16).

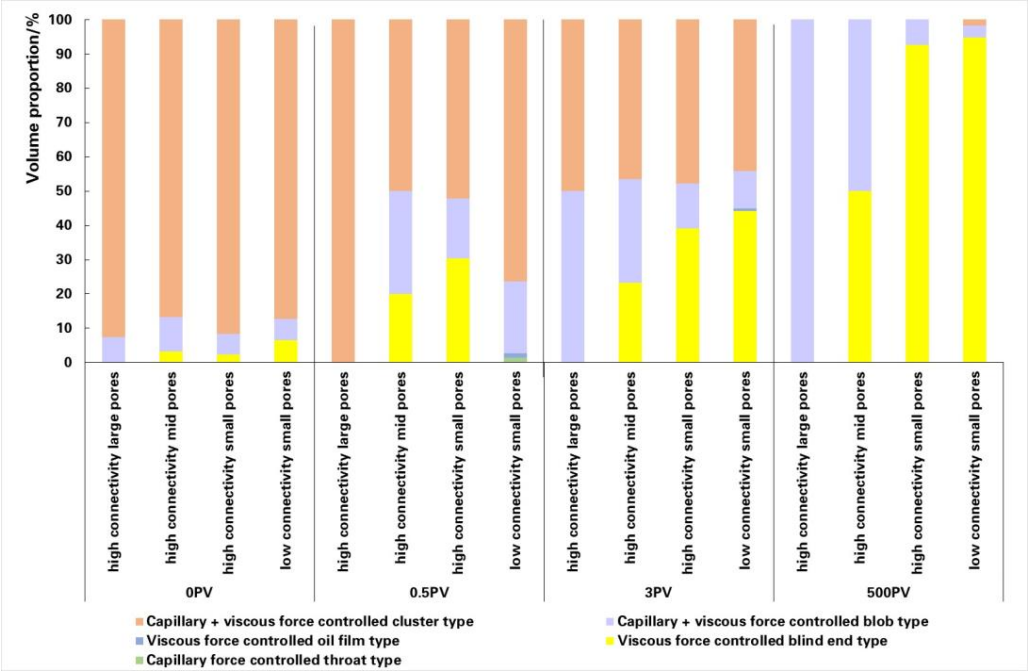

Figure 15. Evolution of microscopic remaining oil in class-III reservoir.

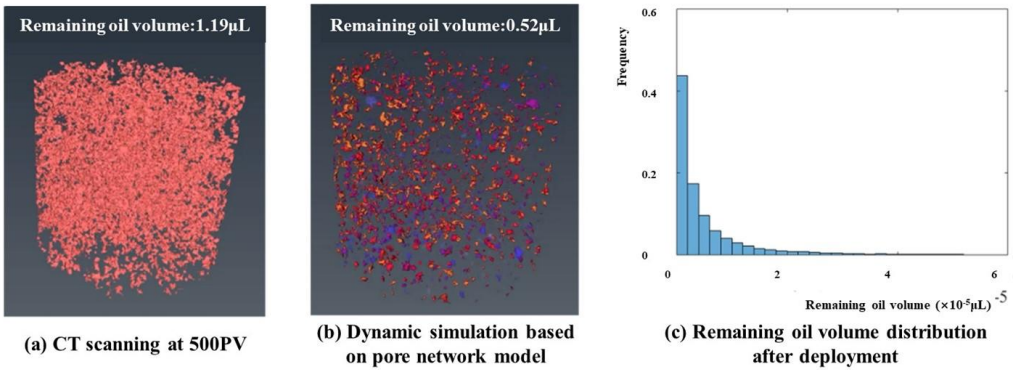

Figure 16. Simulation of micro-remaining oil production in the digital core of class-III oil reservoir.

4. Formation Mechanism and Utilization Conditions

Most remaining oils in the ultra-high water cut stage are dispersed within pores. Therefore, there is a need for a more efficient way to exploit the oil and this is important for improved oil recovery in the ultra-high water cut stage. Similarly, understanding the formation mechanism and utilization conditions of different remaining oils can effectively guide in subsequent water flooding development of oil fields in the ultra-high water cut stage. This indeed is of great significance to achieving increasingly stable and high production in the oilfields.

4.1. Conditions Guiding the Use of Micro-Remaining Oil in Various Reservoirs

Long-term water flooding is usually associated with the fall/plugging of rock particles and the expansion of the clay minerals. These minerals/rock changes lead to the dynamic state of the internal pore structure which has an impact on the flow of the two-phase fluid (water-oil) and utilization of remaining oil. Based on the result of the analyzed core from the CT scan, the pore structure and two-phase fluid displacement process were reconstructed and simulated accordingly. The pore network model is used to simulate the water-oil displacement process in the dynamic pore structure and this is calculated as follows: (1) digital core with pore structure in addition to digital core with spatial distribution of

water and oil are extracted based on CT core data in saturated oil state; (2) using a 0.5 PV, 1 PV, 3 PV, 10 PV, 50 PV and 500 PV CT scan core data set at different displacement stages, the pore structure digital core was extracted; (3) the digital core with saturated pore structures in addition to spatial distribution of water and oil are the initial conditions to be considered. Hence, the core inlet was injected with a constant flow rate of 13 μL/min, 39 μL/min and 130 μL/min at different injection rates (the experimental conditions have to be repeated consistently). (4) At the end of different displacements stages, as the core pore structure is being recorded, the pore network models are extracted. The next stage of water–oil displacement simulation was carried out under the same conditions of spatial distribution of water and oil until 500 PV was attained. When this is combined with the dynamic change in digital pore structure at high-power water flooding, a two-phase numerical simulation of pore scale water-oil displacement can be achieved. This is based on the fluid-solid coupling method, as well as analyzing and evaluating the conditions of the remaining oil production in different types of oil reservoirs during the ultra-high water cut period.

4.2. Utilization Conditions in the Water Flooding Process

4.2.1. Utilization Conditions of Classified Oil Reservoir

The current study provides information on the utilization conditions for classified oil reservoirs at the ultra-high water cut stage. This is based on the analyses of force and morphological characteristics of different types of micro-remaining oil.

Class-I reservoir. Based on the displacement experiment of Sample-1 from the Class-I reservoir, it has been observed that the dominant type of microscopic remaining oil in the Class-I reservoir is the B-type. The microscopic force is driven by positive pressure with viscous force, while it is resisted by the capillary force. It is key to note that, the main driving force (positive pressure) causes the morphological characteristics of microscopic remaining oil to exhibit low water–oil interface connectivity, small water–oil area ratio and small oil–body surface ratio. Therefore, it can be inferred that the positive pressure can be increased by enhancing the displacement velocity or increasing the pressure gradient. On the other hand, the capillary force can be weakened by decreasing interfacial tension to break the dynamic equilibrium state of the microscopic remaining oil and promote the production of B-type microscopic remaining oil. To verify the effectiveness of these measures, the displacement velocity was changed to 260 μL/min while reducing the surface tension to 1 mN/m during the simulation. Figure 12b shows the morphology of the microscopic remaining oil after dynamic simulation. Note that, different colors represent the saturation of the microscopic remaining oil in different pore spaces. When the distribution of the two phases (water and oil) reached a stable state, a marked difference was recorded between the total volume of the microscopic remaining oil (0.17 μL) and the volume of the remaining oil before use (1.38 μL). The displacement efficiency increased by 21% after the implementation of the operation measures. In addition, the volume of the micro-remaining oil in the digital core ranges from 10 to 5 μL, with an average equivalent diameter of 21 μm. This is responsible for the observed great reduction in volume and shape of the studied micro-remaining oil.

Class-II reservoir. Based on the displacement experiment of sample-3 from the Class-II reservoir, the dominant type of microscopic remaining oil in the class-II reservoir is A-type. Its microscopic force is characterized by a complex mixture of positive pressure, viscous force and capillary force. This form of reservoir has a low sweep degree of injected water which causes high water-oil interface connectivity of the microscopic remaining oil. Thus, it can be inferred that the dominant water flooding channel in the core can be controlled by improving the hydrophilicity, increasing the pressure gradient or conducting profile control and water plugging. This is to increase the positive pressure and break the dynamic balance of the oil as it promotes the production of A-type microscopic remaining oil. To verify the effectiveness of this procedure, the wettability and contact Angle (23°) were adjusted during the simulation. The resulting microscopic remaining oil morphology after

dynamic simulation is shown in Figure 14b. At the end, when the two-phase distribution of water and oil attained a stable state, the overall microscopic remaining oil was reduced to 0.26 μL. Compared with the remaining oil volume of 1.75 μL before production, the displacement efficiency after production measures has increased by 28.3%. Furthermore, the volume of the micro-remaining oil in the digital core (0.56×10^{-5} μL) with an average equivalent diameter of 17 μm shows a significant reduction in the volume and shape of the oil.

Class-III reservoir. Based on the displacement experiment of Sample-4 from the Class-III reservoir, the dominant type of microscopic remaining oil in the class-II reservoir is E-type. The microscopic force is driven by positive pressure and resisted by capillary force. Morphologically, it is characterized by low water-oil interface connectivity, small water-oil area ratio and large oil-body surface ratio. For this class, it can be inferred that the positive pressure can be increased via high driving force, while the capillary force can be weakened by reducing the surface tension. This is necessary to break the dynamic equilibrium of the microscopic remaining oil and promote the production of the E-type oil. The effectiveness of these measures can be verified by reducing the surface tension of the fluid to 1 mN/m during the simulation. Figure 16b shows the microscopic remaining oil morphology after dynamic simulation. A close look reveals that, after the two-phase distribution of water and oil gets to a stable state, the overall microscopic remaining oil has reduced to 0.52 μL. When compared with the remaining oil volume before deployment (1.19 μL), the displacement efficiency after the deployment has increased by 17.5%. Moreover, the volume of the microscopic remaining oil in the digital core after production is about 0.9×10^{-5} μL in Figure 16b, with an average equivalent diameter of 20 μm, meaning that the volume of the microscopic remaining oil in the digital core was greatly reduced.

4.2.2. Tapping Method in Ultra-High Water Cut Period

During the high-water cut exploitation stage, the remaining oil clusters exist in discontinuous states such as oil clusters and oil droplets. This is the point at which the remaining oil clusters attain local force balance and do not move easily. Therefore, based on the occurrence state and force characteristics of different types of micro-remaining oil, the potential exploitation directions are determined along with their countermeasures as presented in Table 5 [39,40].

Table 5. Tapping methods for different types of micro-remaining oil.

Type	Cluster Type	Oil Drop Type	Columniform	Film Type	Caeco-Terminal Type
Formation mode	Capillary force + Viscous force		Capillary force	Viscous force	
Use mechanism	Dynamic pressure > Capillary force + viscous force		Dynamic pressure > Capillary force + viscous force	Tangential viscosity > Wall viscosity	
Direction of operation	Increased pressure gradient	Reduce capillary resistance	Increase driving force	Reduce interfacial tension	Increase shear force
Potential exploitation direction	Enhanced injection and production	Change the flow direction	Reservoir reconstruction	Chemical flooding	Improve speed and viscoelasticity

Increasing liquid is effective in improving the utilization degree of A-type remaining oil. The microscopic simulation of porous media indicates that the remaining oil can be partially moved after enhancing the injection velocity. This is subject to if it has not been produced at the final stage of the first water flooding. At higher speed and stronger water driving force, the stability of the oil–water phase interface was altered. Thus, the flow resistance of the remaining oil decreases when the remaining oil breaks at the small pore throat. This allows the water phase into the larger pore channel and forces the remaining oil to flow.

The main effect of increasing liquid is to change the dynamic pressure in the pore space during this process of utilization. In the late stage of the first water flooding, the

stability of the dynamic pressure (at about 0.06 MPa), does not allow the formation of an effective driving pressure difference. The water driving force was enhanced by increasing the injection flow rate to increase the dynamic pressure from 0.18 MPa to 0.35 MPa during the secondary water flooding. This pushed the oil–water phase interface to move and cut off the original porous remaining oil, hence, part of the A-type remaining oil was made to migrate (Figure 17).

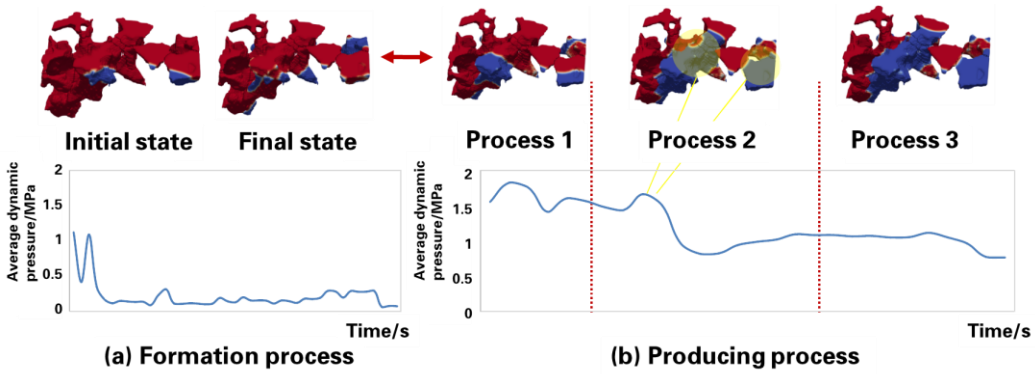

Figure 17. Formation and utilization process of A-type remaining oil by dynamic pressure change.

Change of water flow direction is effective in improving the utilization degree of B-type remaining oil. The B-type remaining oil that was not used in the final stage of the first water flooding migrated effectively after the change of flow direction. The change of flow direction leads to an effective driving pressure difference, which promotes the deformation of the phase interface. This process will bring about a change in the shape of the remaining oil and lead to the formation of a new interface; thus, part of the B-type remaining oil was extracted as shown in Figure 18.

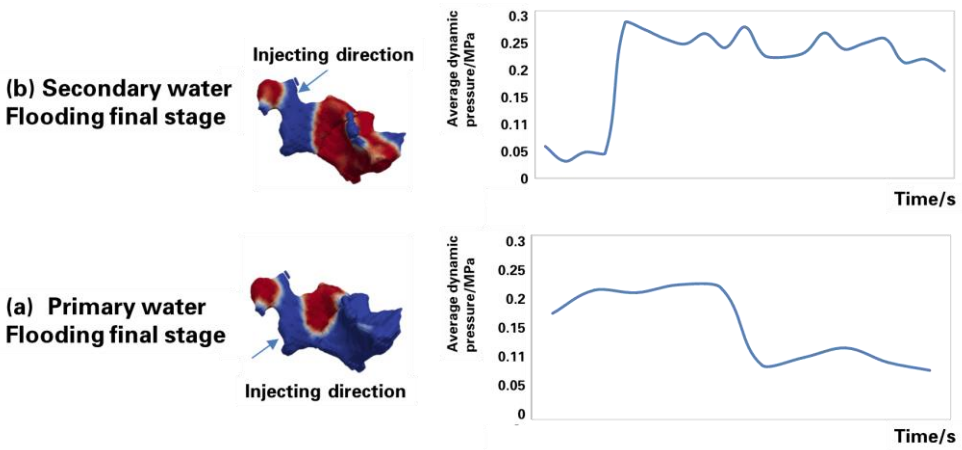

Figure 18. Formation and utilization process of B-type remaining oil by dynamic pressure change.

5. Conclusions

(i) Four rock samples from 3 oil formations were subjected to an integrated displacement CT scanning involving high-end equipment (Xradia MicroXCT-400 micro-CT) at 8 displacement nodes with a scanning accuracy of 1.91 μm. This study aims to investigate the classification method, state of occurrence and utilization mechanism of microscopic remaining oil in the late period of ultra-high water cut.

Generally, the experimental results reveal the characteristics of different production stages, and the guiding rule is that the displacement speed increases from 13 μL/min to 39 μL/min. An increase in the pore volume from 3 PV to 10 PV brings a great improvement in the degree of recovery. It has to be noted that, although displacement efficiency continues to rise from 10–50 PV, change in the degree of recovery slows down after 50 PV.

(ii) This study employs a mechanical mechanism to establish a classification method for the microscopic remaining oil. The classification limit was determined by selecting three basic parameters which were related to the forces of oil–water connectivity, the specific surface of the oil mass and the area ratio of the oil to water. Based on this, here are the five types of the microscopic remaining oil: A-type (capillary + viscous control cluster), B-type (capillary + viscous oil drop), C-type (viscous control oil film), D-type (capillary control throat), and E-type (viscous control blind end).

(iii) The microscopic remaining oil occurrence state of various oil layers with different pore structures in the late period of ultra-high-water cut were differentiated into three types. The first type has predominantly capillary + viscous oil droplet type distributed in large pores with high connectivity. Capillary + viscous oil cluster type dominates the second type of oil layer. It is mainly distributed in small and medium pores with high connectivity. Where the oil layer is supported by the capillary force-controlled throat type represents the third type. This is mainly distributed in highly connected pores.

(iv) Based on the result of this study, several potential exploitation methods for micro-remaining oil have been formulated. The main potential exploitation directions are defined on the basis of the stress analysis of different micro-remaining oils. Also identified as a critical factor is the effective means such as increasing the pressure gradient of liquid extraction and changing the direction of liquid flow. An effective way to improve the remaining oil utilization is to increase the pressure gradient and change the direction of liquid flow during the water-drive development process. The right combination of these factors is important to improve the degree of utilization of micro-remaining oil, as it provides a theoretical basis for the deep development in the late period of ultra-high water cut.

Author Contributions: Conceptualization, Y.H.; Methodology, X.Z., J.W. (Jiayi Wu) and W.G.; Validation, J.W. (Jiayi Wu), J.W. (Jiawen Wu) and Z.W.; Resources, X.Z., Y.H. and Q.W.; Data curation, Q.W. and X.G.; Writing—original draft, Y.H., X.Z. and J.W. All authors have read and agreed to the published version of the manuscript.

Funding: This work is financially supported by the Scientific Research and Technology Development Projects of PetroChina (2023ZZ22YJ02).

Data Availability Statement: Data is contained within the article.

Conflicts of Interest: Authors Yuhang He, Xianbao Zheng, Jiayi Wu, Zhiqiang Wang, Qingyu Wang and Xuecong Gai were employed by the company PetroChina. The remaining authors declare that the research was conducted in the absence of any commercial or financial relationships that could be construed as a potential conflict of interest. The authors declare that this study received funding from PetroChina. The funder was not involved in the study design, collection, analysis, interpretation of data, the writing of this article or the decision to submit it for publication.

References

1. Hou, Q.; He, H.-Q.; Li, J.; Yang, T. Recent progress and prospect of oil and gas exploration by PetroChina Company Limited. *China Pet. Explor.* **2018**, *23*, 1–13.
2. Zhang, N.; Wang, Q.; Wang, J.; Hou, L.; Li, H.; Li, Q. Characteristics of oil and gas discoveries in recent 20 years and future exploration in the world. *Pet. Explor. Dev.* **2018**, *23*, 44–53.
3. Chan, H.; Shi, C.; Hu, H.; Wu, H.; Chen, C. Advances in fine description of reservoir in high water-cut oilfield. *Oil Gas Geol.* **2018**, *39*, 1311–1322.
4. Chen, H. Progress in the fine description of reservoirs in China and its prospect. *Geol. China* **2021**, *48*, 424–446.
5. Du, Q.; Song, B.; Zhu, L.; Jiang, Y.; Zhao, G. Challenges and countermeasures of the waterflooding development for Lasaxing oilfields during extra-high watercut period. *Pet. Geol. Oilfield Dev. Daqing* **2019**, *38*, 189–194.
6. Cui, C.; Li, S.; Yang, Y.; Wang, J.; Huang, Y.; Wu, Z. Zonal Regulation method for reservoirs in ultra-high water cut stage. *Acta Pet. Sin.* **2018**, *39*, 1155–1161.
7. Zhu, L.; Wang, H.; Wei, L.; Guo, J. Quantitative identification of the low and no-efficiency cycle fields based on CRM. *Oilfield Dev. Daqing* **2019**, *38*, 239–245.
8. Du, Q. Variation law and microscopic mechanism of permeability in sandstone reservoir during long-term water flooding development. *Acta Pet. Sin.* **2016**, *37*, 1159–1164.

9. Ju, Y.; Gong, W.; Chang, W.; Sun, M. Effects of pore characteristics on water-oil two-phase displacement in non-homogeneous pore structures: A pore-scale lattice Boltzmann model considering various fluid density ratios. *Int. J. Eng. Sci.* **2020**, *154*, 103343. [CrossRef]
10. Lei, W.; Liu, T.; Xie, C.; Yang, H.; Wu, T.; Wang, M. Enhanced oil recovery mechanism and recovery performance of micro-gel particle suspensions by microfluidic experiments. *Energy Sci. Eng.* **2020**, *8*, 986–998. [CrossRef]
11. Yan, W.; Sun, J. Analysis of research present situation of microscopic remaining oil. *Prog. Geophys.* **2016**, *31*, 2198–2211.
12. Alhosani, A.; Bijeljic, B.; Blunt, M.J. Pore-scale imaging and analysis of wettability order, trapping and displacement in three-phase flow in porous media with various wettabilities. *Transp. Porous Media* **2021**, *140*, 59–84. [CrossRef]
13. Ju, Y.; Xi, C.; Zheng, J.; Gong, W.; Wu, J.; Wang, S.; Mao, L. Study on three-dimensional immiscible water–Oil two-phase displacement and trapping in deformed pore structures subjected to varying geostress via in situ computed tomography scanning and additively printed models. *Int. J. Eng. Sci.* **2022**, *171*, 103615. [CrossRef]
14. Li, Y.; Zhang, J.; Pan, D.; Yan, Y.; Liu, M.; Cao, H.; Gao, W. Occurrence Laws of Microscopic Remaining Oil in High Water-Cut Reservoirs: A Case Study on Blocks Xiaoji and Gangxi in Dagang Oilfield. *Xinjiang Pet. Geol.* **2021**, *42*, 444–449.
15. Sun, Y.; Lin, C.; Wang, L. Microscopic formation mechanisms and distribution patterns of remaining oil in the marine clastic reservoirs of the Carboniferous, Tarim Basin. *Oil Gas Geol.* **2021**, *42*, 1334–1343.
16. Wang, C.; Jiang, H.; Xu, F.; Yu, F.; Zhao, Y.; Li, J. Study of the variation of pore-scale residual oil flow based on a microfluidic model. *Pet. Sci. Bull.* **2020**, *5*, 376–391.
17. Liu, Y.; Dong, X.; Chen, Z.; Hou, Y.; Luo, Q.; Chen, S. Pore-scale movability evaluation for tight oil enhanced oil recovery methods based on miniature core test and digital core construction. *Ind. Eng. Chem. Res.* **2021**, *60*, 2625–2633. [CrossRef]
18. Jiang, N.; Zhang, Z.; Qu, G.; Zhi, J.; Zhang, R. Distribution Characteristics of Micro Remaining Oil of Class III Reservoirs after Fracture Flooding in Daqing Oilfield. *Energies* **2022**, *15*, 3385. [CrossRef]
19. Zhang, L.; Nie, J.; Yu, H. Countermeasures of producing for microcosmic residual oil in ultra-high water cut stage. *Sino-Glob. Energy* **2021**, *26*, 44–48.
20. Pei, X.; Su, Y.; Yu, J. Study on Pore Structure and Microscopic Remaining Oil Distribution Characteristics of Type-II Oil Reservoirs in Lmd Oilfield. *Sino-Glob. Energy* **2023**, *28*, 38–45.
21. Cai, H. Study on reasonable injection-production control limit based on the change law of microcosmic residual oil start-up conditions. *China Offshore Oil Gas* **2023**, *35*, 94–102.
22. Gao, W.; Li, Y.; He, S.; Pan, D. Classification method of occurrence mode of remaining oil based on fluorescence thin sections. *Acta Pet. Sin.* **2020**, *41*, 1406–1415.
23. Su, Y.; Zha, M.; Jiang, L.; Ding, X.; Qu, J.; Jin, J.; Iglauer, S. Pore structure and fluid distribution of tight sandstone by the combined use of SEM, MICP and X-ray micro-CT. *J. Pet. Sci. Eng.* **2022**, *208*, 109241. [CrossRef]
24. Yang, Y.; Xiao, W.; Bernabe, Y.; Xie, Q.; Wang, J.; He, Y.; Li, M.; Chen, M.; Ren, J.; Zhao, J.; et al. Effect of pore structure and injection pressure on waterflooding in tight oil sandstone cores using NMR technique and pore network simulation. *J. Pet. Sci. Eng.* **2022**, *217*, 110886. [CrossRef]
25. Guo, C.; Wang, X.; Wang, H.; He, S.; Liu, H.; Zhu, P. Effect of pore structure on displacement efficiency and oil-cluster morphology by using micro-computed tomography (μCT) technique. *Fuel* **2018**, *230*, 430–439. [CrossRef]
26. Jia, Z.; Yuan, M.; Yuan, M.; Zhang, X.; Dong, J.; Yang, Q. Waterflooding microscopic flow characteristics and the remained oil starting mechanisms. *Pet. Geol. Oilfield Dev. Daqing* **2018**, *37*, 65–70.
27. Bai, Z.; Wang, Q.; Li, Y. Distribution law of microscopic remaining oil in polymer-flooded reservoirs of sandstone oilfield. *Pet. Geol. Oilfield Dev. Daqing* **2021**, *40*, 101–106.
28. Li, J.; Jiang, H.; Wang, C.; Zhao, Y.; Gao, Y.; Pei, Y.; Wang, C.; Dong, H. Pore-scale investigation of microscopic remaining oil variation characteristics in water-wet sandstone using CT scanning. *J. Nat. Gas Sci. Eng.* **2017**, *48*, 36–45. [CrossRef]
29. Gong, W.; Liu, Y.; Xi, C.; Yang, G.; Ju, Y.; Wang, M. Dynamic characterization of residual oil during long-term waterflooding experiments in heterogeneous porous structures. *Fuel* **2024**, *356*, 129567. [CrossRef]
30. Fang, Y.; Yang, E.; Guo, S.; Cui, C.; Zhou, C. Study on micro remaining oil distribution of polymer flooding in Class-II B oil layer of Daqing Oilfield. *Energy* **2022**, *254*, 124479. [CrossRef]
31. Spurin, C.; Bultreys, T.; Ruecker, M.; Garfi, G.; Schlepütz, C.M.; Novak, V.; Berg, S.; Blunt, M.J.; Krevor, S. Real-time imaging reveals distinct pore-scale dynamics during transient and equilibrium subsurface multiphase flow. *Water Resour. Res.* **2020**, *56*, e2020WR02828. [CrossRef]
32. Wu, Y.; Tahmasebi, P.; Liu, K.; Fagbemi, S.; Lin, C.; An, S.; Ren, L. Two-phase flow in heterogeneous porous media: A multiscale digital model approach. *Int. J. Heat Mass Transf.* **2022**, *194*, 123080. [CrossRef]
33. *GB/T 29172-2012*; Practices for Core Analysis. AQSIQ & Standardization Administration of China: Beijing, China, 2012.
34. Qin, X.; Xia, Y.; Wu, J.; Sun, C.; Zeng, J.; Xu, K.; Cai, J. Influence of Pore Morphology on Permeability through Digital Rock Modeling: New Insights from the Euler Number and Shape Factor. *Energy Fuels* **2022**, *36*, 7519–7530. [CrossRef]
35. Liu, Y.; Gong, W.; Xiao, H.; Wang, M. A pore-scale numerical framework for solute transport and dispersion in porous media. *Adv. Water Resour.* **2024**, *183*, 104602. [CrossRef]
36. Liu, Y.; Gong, W.; Zhao, Y.; Jin, X.; Wang, M. A Pore-throat segmentation method based on local hydraulic resistance equivalence for pore-network modeling. *Water Resour. Res.* **2022**, *58*, e2022WR033142. [CrossRef]

37. Bugni, F.A.; Canay, I.A. Testing continuity of a density via g-order statistics in the regression discontinuity design. *J. Econom.* **2021**, *221*, 138–159. [CrossRef]
38. Sun, P.; Xu, H.; Zhu, H.; Jia, L.; Hu, X.; Fang, H.; Jiang, H.; Xu, Z.; Jiang, T.; Jiang, X.; et al. Investigation of pore-type heterogeneity and its control on microscopic residual oil distribution in deeply buried marine clastic reservoirs. *Mar. Pet. Geol.* **2021**, *123*, 104750. [CrossRef]
39. Wang, F.; Liu, T.; Lei, W.; Zhao, Y.; Li, B.; Yang, G.; Liu, Y.; Wang, M. Dynamic analysis of deformation and start-up process of residual-oil droplet on wall under shear flow. *J. Pet. Sci. Eng.* **2021**, *199*, 108335. [CrossRef]
40. Guo, J.; Yang, E.; Zhao, Y.; Fu, H.; Dong, C.; Du, Q.; Zheng, X.; Wang, Z.; Yang, B.; Zhu, J. A New Method for Optimizing Water-Flooding Strategies in Multi-Layer Sandstone Reservoirs. *Energies* **2024**, *17*, 1828. [CrossRef]